Gravitational lens equation for embedded lenses; magnification and ellipticity

B. Chen, R. Kantowski, and X. Dai

The Gravitational Lens Equation for Embedded Lenses; Magnification and Ellipticity

B. Chen,[1,2,*] R. Kantowski,[1,†] and X. Dai[1,‡]

[1]*Homer L. Dodge Department of Physics and Astronomy,*

University of Oklahoma, 440 West Brooks, Norman, OK 73019, USA

[2]*Mathematics Department,University of Oklahoma,*

601 Elm Avenue, Norman, OK 73019, USA

Abstract

We give the lens equation for light deflections caused by point mass condensations in an otherwise spatially homogeneous and flat universe. We assume the signal from a distant source is deflected by a single condensation before it reaches the observer. We call this deflector an embedded lens because the deflecting mass is part of the mean density. The embedded lens equation differs from the conventional lens equation because the deflector mass is not simply an addition to the cosmic mean. We prescribe an iteration scheme to solve this new lens equation and use it to compare our results with standard linear lensing theory. We also compute analytic expressions for the lowest order corrections to image amplifications and distortions caused by incorporating the lensing mass into the mean. We use these results to estimate the effect of embedding on strong lensing magnifications and ellipticities and find only small effects, $< 1\%$, contrary to what we have found for time delays and for weak lensing, $\sim 5\%$.

I. INTRODUCTION

Conventional extragalactic gravitational lensing assumes that the Universe is homogeneous and isotropic on scales significantly smaller than observer/source/deflector distances, i.e., that the cosmological principal applies at these distances. It also assumes that a lensing inhomogeneity such as a galaxy or cluster of galaxies is an addition to the homogeneous mean. What we investigate here is the extent to which errors are made because of this latter assumption. To assume a single galaxy is an addition to the mean might not seem irrational but to assume giant super clusters are is more suspect. In fact they are both contributing to the mean and hence do not act as infinite range deflectors. To understand why, one only has to surround a typical deflector by an imaginary sphere of radius r and note that the average mass density inside the sphere decreases as r increases until the density reaches the cosmological mean at some $r=r_b$. If this were not correct the cosmological principle would

* bin.chen-1@ou.edu

† kantowski@nhn.ou.edu

‡ xdai@ou.edu

be in error. Beyond the gravitational boundary r_b, the gravitational field has returned to the homogeneous mean and the lens ceases to produce any additional deflection of a passing light ray. In this paper we compute modifications to the lens equation caused by this finite range. To make sure we properly account for the lensing gravity we use an exact solution to Einstein's equations. We assume the deflector is a simple point mass lens embedded in a flat Friedman-Lemaître-Robertson-Walker (FLRW) universe, see Eq. (1), whose energy content includes pressureless dust (cold dark matter) and a cosmological constant Λ ($\Omega_{\mathrm{m}} + \Omega_{\Lambda} = 1$). The mathematics of the embedding process is the same as embedding in the Swiss cheese cosmological models [1–4]. These models are the only known exact general relativistic (GR) solutions which embed spherical inhomogeneities into homogeneous background universes. The range r_b above is given by the comoving radial boundary of the homogeneous sphere that has been replaced by the condensation. Beyond that boundary the gravity caused by a condensation and a homogeneous sphere are exactly the same. Schücker [5] refers to this radius as the Schücking radius. For a point mass lens the removed dust sphere of comoving radius χ_b is replace by a Kottler condensation [6], i.e., Schwarzschild with a cosmological constant, see Eq. (2). This complete condensation of mass is often criticized on aesthetic grounds. The jump in mass density at the boundary of the void is obviously nonphysical; however, the model's optical properties appropriately correct for embedded inhomogeneities (see [7, 8] for more details about optics in, references for, and history of this model). The discontinuities do not cause refraction and just as in conventional linear lensing the mean density of the mass in the light beam is the important quantity, not its actual discontinuous distribution along the beam. In [7, 9] we derived analytical expressions for the bending angle α and the time delay ΔT of a photon that encounters such a condensation. Related work appeared in [10–15]. In this paper we derive the embedded lens equation and prescribe a scheme to iteratively solve it.

The flat FLRW metric for the background cosmology can be written as

$$ds^2 = -c^2 dT^2 + R(T)^2 \left[d\chi^2 + \chi^2 (d\theta^2 + \sin^2 \theta d\phi^2) \right], \tag{1}$$

and the embedded condensation is described by the Kottler or Schwarzschild-de Sitter metric [6] which can be written as

$$ds^2 = -\gamma(r)^{-2} c^2 dt^2 + \gamma(r)^2 dr^2 + r^2 (d\theta^2 + \sin^2 \theta \, d\phi^2), \tag{2}$$

3

where $\gamma^{-1}(r) \equiv \sqrt{1 - \beta^2(r)}$ and $\beta^2(r) \equiv r_s/r + \Lambda r^2/3$. The constants r_s and Λ are the Schwarzschild radius $(2Gm/c^2)$ of the condensed mass and the cosmological constant respectively. By matching the first fundamental forms at the Kottler-FLRW boundary, angles (θ, ϕ) of Eqs. (2) and (1) are identified and the expanding Kottler radius r_b of the void is related to the comoving FLRW radius χ_b by

$$r_b = R(T)\chi_b. \tag{3}$$

By matching the second fundamental forms the Schwarzschild radius r_s of the Kottler condensation is related to FLRW by

$$r_s = \Omega_{\mathrm{m}} \frac{H_0^2}{c^2} (R_0 \chi_b)^3, \tag{4}$$

where H_0 is the Hubble constant and the cosmological constant Λ is constrained to be the same inside and outside of the Kottler hole.

In Section II we give the lens equation valid for deflections caused by Kottler condensations in the flat FLRW universe and numerically compare its predictions with conventional lensing theory for a source at redshift one and a deflector at redshift one half. In Section III we give analytic expressions for image magnifications and distortions for the embedded point mass lens (to lowest order only) and compare them with conventional lensing results.

II.   THE LENS EQUATION

The Swiss cheese lensing geometry is shown in Fig. 1. The deflected photon leaves a source S, enters a Kottler hole at point 1, exits at point 2 with a deflection angle $\alpha < 0$, and then proceeds to the observer at O. Point B is the intersection of the forward and backward extensions of respective FLRW rays $S1$ and $2O$ drawn as if the Kottler hole were absent and the original ray was simply reflected at point B. Angles θ_I and θ_S are respectively the image and source positions relative to the observer-deflector optical axis OD. The rotation angle ρ measures the difference between the horizontal axis [with respect to which we measure the spherical polar angle ϕ, see Eqs. (2) and (14) and Fig. 1] and the optical axis. A negative ρ is a clockwise rotation of the observer. The lens equation for a given deflector mass and background cosmology is simply the equation that gives θ_I as a function of θ_S for fixed comoving source-observer distance χ_s and deflector-observer distance χ_d, and fixed photon
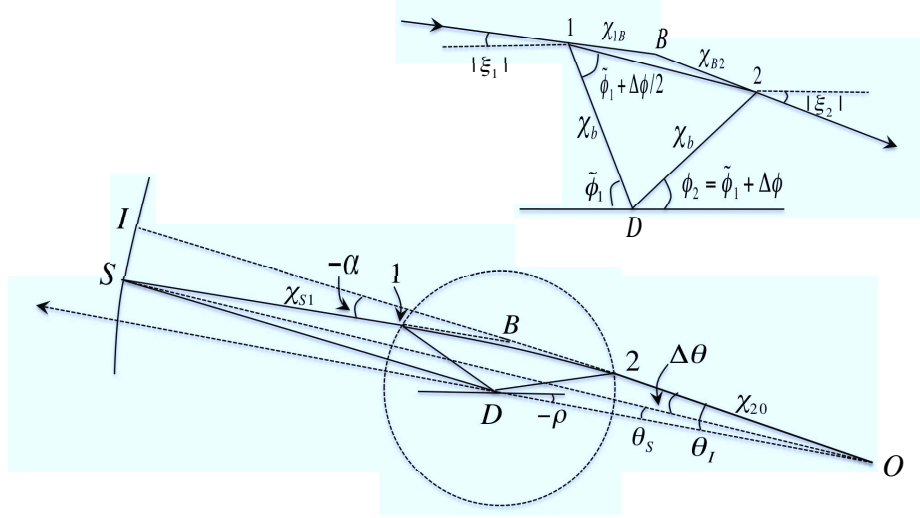
4

FIG. 1. The comoving embedded lensing geometry. Points S, D and O represent respectively the source, deflector, and observer positions. The point B is a fictitious reflection point. Points 1 and 2 denote the photon's entrance and exit from the Kottler void. The bending angle is α, θ_I and θ_S are respectively the image and source position angles at the observer measured relative to the optical axis OD, and $\Delta\theta \equiv \theta_I - \theta_S$. A similar geometry appears in Fig. 1 of [7]. The figure represents the $\theta = \pi/2$ plane (the plane containing the photon's orbit) of the spherical polar coordinates used in Eqs. (1) and (2). The ϕ orientation is fixed by requiring the photon's point of closest approach to the Schwarzschild mass, r_0, occur at $\phi = \pi/2$.

arrival time T_O. For non-embedded lenses, i.e., for conventional linear lensing theory, this relation is straightforward to obtain even for complicated lensing mass profiles, because the deflector is completely unrelated to the cosmology. For an embedded lens this is no longer the case. However, because of the azimuthal symmetry of the lensing geometry all photon orbit variables can be thought of as depending on a single independent variable. Choosing θ_S or the photon's minimum Kottler coordinate r_0 would be logical but not convenient. In what follows we have chosen to give all quantities as functions of $\tilde{\phi}_1$ where $\pi - \tilde{\phi}_1$ is the azimuthal angle of the photon at entry into the Kottler void (see Fig. 1, or Fig. 1 of [7]). Because $r_0(\tilde{\phi}_1)$ is a complicated function, r_0 is retained in all expressions and only evaluated when needed.

The embedded lens equation can be obtained by applying the law of sines to the triangle SBO of Fig. 1

$$\sin(\theta_S - \theta_I - \alpha) = \frac{\chi_{BO}}{\chi_s} \sin(-\alpha). \tag{5}$$

5

The embedded lens equation can be compared to the standard linear lensing equation [16, 17] for flat FLRW

$$\theta_S - \theta_I = -\frac{D_{ds}}{D_s}(-\alpha) = -\frac{\chi_s - \chi_d}{\chi_s}(-\alpha), \tag{6}$$

where small angle approximations are made and the differences between distances from the observer to the deflector and to the reflection point B (χ_d and χ_{BO}) are neglected. Since we are now computing the linear and non-linear corrections to the standard lensing theory, we cannot make such simplifications as is done in [18] and [19]. To find the relation between these two distances we apply the law of sines to the comoving triangle $D2O$,

$$\begin{aligned}\chi_{2O} &= \frac{\sin(\phi_2 - \xi_2 - \theta_I)}{\sin(\phi_2 - \xi_2)}\chi_d \\ &= \left[\cos\theta_I - \cos(\phi_2 - \xi_2)\frac{\sin\theta_I}{\sin(\phi_2 - \xi_2)}\right]\chi_d.\end{aligned} \tag{7}$$

Applying the law of sines to the comoving triangle $D2O$ again and noting that $\phi_2 = \tilde{\phi}_1 + \Delta\phi$, $\xi_2 = \xi_1 + \alpha$ by definition, we obtain

$$\chi_{2O} = \left[\cos\theta_I - \cos(\tilde{\phi}_1 - \xi_1 + \Delta\phi - \alpha)\frac{\chi_b}{\chi_d}\right]\chi_d, \tag{8}$$

where χ_b, the Kottler void radius [see Eq. (4)], is assumed known. The angles ξ_1, $\xi_2 = \xi_1 + \alpha$, $\tilde{\phi}_1$, and $\Delta\phi$ are exhibited in Fig. 1 and are the same as those used in [7, 9] where analytic expansions for them as explicit functions of r_0 and $\tilde{\phi}_1$ can be found. The angles ξ_1 and ξ_2 are negative and give the respective slopes of the photon as it enters the Kottler hole at azimuthal angle $\pi - \tilde{\phi}_1$ and exits at angle $\phi_2 = \Delta\phi + \tilde{\phi}_1$ (see Fig. 1 of [7]). The comoving distance χ_{B2} can be obtained from trig identities applied to triangles $1B2$ and $1D2$ of Fig. 1

$$\chi_{B2} = -2\frac{\sin(-\Delta\phi/2 + \xi_1)}{\sin\alpha}\cos\left(\tilde{\phi}_1 + \frac{\Delta\phi}{2}\right)\chi_b. \tag{9}$$

Combining this with Eq. (8) we obtain the relation of χ_{BO} to χ_d,

$$\begin{aligned}\chi_{BO} &\equiv \chi_{2O} + \chi_{B2} \\ &= \left\{\cos\theta_I - \left[\cos(\tilde{\phi}_1 - \xi_1 + \Delta\phi - \alpha) \right.\right. \\ &\quad \left.\left. +\frac{2\sin(-\Delta\phi/2 + \xi_1)}{\sin\alpha}\cos\left(\tilde{\phi}_1 + \frac{\Delta\phi}{2}\right)\right]\frac{\chi_b}{\chi_d}\right\}\chi_d \\ &\equiv g(\theta_I, \xi_1, \Delta\phi, \alpha)\chi_d.\end{aligned} \tag{10}$$

The new lens equation (5) becomes

$$\theta_S = \theta_I + \alpha + \sin^{-1}\left[\frac{\chi_d}{\chi_s}\, g(\theta_I, \xi_1, \Delta\phi, \alpha)\sin(-\alpha)\right], \tag{11}$$

The task at hand is to evaluate all variables on the right hand side of Eq. (11) as functions of a common variable e.g., $\tilde{\phi}_1$. Once accomplished, $\theta_S(\tilde{\phi}_1)$ and $\theta_I(\tilde{\phi}_1)$ can be tabulated to give the desired image position as a function of the source position, $\theta_I(\theta_S)$. The image angle θ_I can be determined from knowledge of ξ_1, $\Delta\phi$, and α by applying the law of sines to the triangle $D2O$

$$\sin\theta_I = \sin(\tilde{\phi}_1 - \xi_1 + \Delta\phi - \alpha)\frac{\chi_b}{\chi_d}. \tag{12}$$

The bending angle α is given by Eq. (32) of [7], $\Delta\phi \equiv \phi_2 - \tilde{\phi}_1$ is given by Eq. (13) of [9], and the photon's slope angle ξ_1 results from evaluating Eqs. (16)-(19) of [7] at the photon's entry point into the Kottler void (to fourth order)

$$\begin{aligned}
\xi_1 = &-\beta_1 \sin\tilde{\phi}_1 + \frac{m}{r_0}\cos\tilde{\phi}_1(2 + \sin^2\tilde{\phi}_1) - \frac{1}{3}\beta_1\frac{m}{r_0}(6 - 3\sin^2\tilde{\phi}_1 - 2\sin^4\tilde{\phi}_1) \\
&-\frac{1}{18}\beta_1\Lambda r_0^2 \sin\tilde{\phi}_1 - \frac{1}{4}\frac{m^2}{r_0^2}\Big[15(\tilde{\phi}_1 - \frac{\pi}{2}) + \cos\tilde{\phi}_1(8 - 15\sin\tilde{\phi}_1 + 4\sin^2\tilde{\phi}_1 \\
&+14\sin^3\tilde{\phi}_1 + 4\sin^5\tilde{\phi}_1)\Big] + \mathcal{O}(5).
\end{aligned} \tag{13}$$

The rotation angle ρ can be computed from the photon's exiting slope $\xi_1 + \alpha$ and the image position θ_I using

$$\rho = \xi_1 + \alpha + \theta_I \ < 0. \tag{14}$$

The expansion speed $\beta = v/c$ of the void boundary relative to stationary Kottler observers is defined in Eq. (2) and when evaluated at the photon's entry point is called β_1 (see Fig. 1 of [7]). Keeping terms to 4th order is necessary in order to correct point mass time delays for embedding.

In the expressions for $\xi_1, \Delta\phi$, and α, approximation orders have been counted as follows: β_1 is 1st order, r_s/r_0 and Λr_0^2 are both 2nd. All terms are made of sums and/or products of these. The expansion speed β_1 depends on $\tilde{\phi}_1$ and r_0 through its dependence on r_1 (which is given by the symmetric null geodesics of the Kottler metric Eq. (2))

$$\begin{aligned}
r_1 = \frac{r_0}{\sin\tilde{\phi}_1}\Bigg\{&1 + \frac{r_s}{2r_0}\left(1 + \sin\tilde{\phi}_1 - \frac{2}{\sin\tilde{\phi}_1}\right) - \left(\frac{r_s}{2r_0}\right)^2\left[\frac{17}{4} - \frac{1}{4}\sin^2\tilde{\phi}_1 - \frac{4}{\sin^2\tilde{\phi}_1}\right. \\
&\left.+\frac{15}{8}\left(\pi - 2\tilde{\phi}_1\right)\cot\tilde{\phi}_1\right] + \mathcal{O}(6)\Bigg\}.
\end{aligned} \tag{15}$$

The above expansion is valid only when $\sin\tilde{\phi}_1 \gg r_s/r_0$. All quantities on the RHS of the embedded lens equation (11) can now be evaluated as functions of $\tilde{\phi}_1$ and r_0. These two variables fix the photon's symmetric orbit (symmetric about $\phi = \pi/2$) while in the Kottler

hole. They are independent unless the photon is additionally constrained by originating at a specific cosmic source or arriving at a specific observer. To eliminate one of these two variables an additional relation between them such as a cosmic timing constraint must be used. For the photon which started at a fixed χ_s to have reached the observer at time T_O after entering the Kottler void at $\tilde{\phi}_1$ and passing with minimum impact r_0, it must have impacted the Kottler void at a specific time T_1 or equivalently at a specific redshift z_1 $(1 + z_1 = R_0/R(T_1))$. Knowledge of z_1 allows us to independently determine r_1 from the embedding equations (3) and (4) i.e., by using

$$r_1 = \frac{1}{1+z_1}\left(\frac{r_s}{\Omega_{\mathrm{m}}}\frac{c^2}{H_0^2}\right)^{1/3}. \tag{16}$$

Because z_1 is not assumed known we compute $z_1 - z_d$, the difference in entry redshift and the (assumed known) deflector redshift, using techniques similar to those developed in [7, 9]. The result up to fourth order is

$$
\begin{aligned}
z_d - z_1 = (1+z_1)\Big[&\Delta z^{\mathrm{1st}}(z_1, \tilde{\phi}_1) + \Delta z^{\mathrm{2nd}}(z_1, r_0, \tilde{\phi}_1) + \Delta z^{\mathrm{3rd}}(z_1, r_0, \tilde{\phi}_1) \\
&+ \Delta z^{\mathrm{4th}}(z_1, r_0, \tilde{\phi}_1)\Big],
\end{aligned} \tag{17}
$$

where

$$\Delta z^{\mathrm{1st}} = -\beta_1 \cos \tilde{\phi}_1, \tag{18}$$

$$\Delta z^{\mathrm{2nd}} = -\frac{\Lambda r_0^2}{3} + \frac{1}{2}\beta_1 \frac{\chi_b}{\chi_d}\sin^2 \tilde{\phi}_1 + \frac{1}{2}\frac{m}{r_0}\sin \tilde{\phi}_1\left(3 - 7\sin^2 \tilde{\phi}_1\right), \tag{19}$$

$$
\begin{aligned}
\Delta z^{\mathrm{3rd}} = &\frac{1}{6}\beta_1 \Lambda r_0^2 \cos \tilde{\phi}_1 - \frac{\Lambda r_0^2}{3}\frac{\chi_b}{\chi_d}\cos \tilde{\phi}_1 + \frac{1}{3}\beta_1 \frac{m}{r_0}\left[\cos \tilde{\phi}_1\left(7 + 26\sin \tilde{\phi}_1^2\right) + 12\log\tan\frac{\tilde{\phi}_1}{2}\right]\sin \tilde{\phi}_1 \\
&-\frac{7}{2}\frac{m}{r_0}\frac{\chi_b}{\chi_d}\cos \tilde{\phi}_1 \sin^3 \tilde{\phi}_1,
\end{aligned} \tag{20}
$$

and

$$
\begin{aligned}
\Delta z^{\mathrm{4th}} = &\frac{1}{6}\beta_1 \Lambda r_0^2 \frac{\chi_b}{\chi_d}(1 - 2\sin \tilde{\phi}_1^2) + \frac{1}{2}\beta_1 \frac{\chi_b}{\chi_d}\frac{m}{r_0}\left(4 + 9\sin \tilde{\phi}_1^2 - 18\sin \tilde{\phi}_1^4\right)\sin \tilde{\phi}_1 + \frac{1}{8}\beta_1\left(\frac{\chi_b}{\chi_d}\right)^3 \sin^4 \tilde{\phi}_1 \\
&+ \frac{3}{8}\frac{m}{r_0}\left(\frac{\chi_b}{\chi_d}\right)^2 \sin^5 \tilde{\phi}_1 - \frac{1}{36}\frac{m}{r_0}\Lambda r_0^2 \csc \tilde{\phi}_1\Big(61 + 24\sin \tilde{\phi}_1 + 124\sin \tilde{\phi}_1^2 - 227\sin \tilde{\phi}_1^4 \\
&+ 48\cos \tilde{\phi}_1 \log\tan\frac{\tilde{\phi}_1}{2}\Big) + \frac{1}{12}\frac{m^2}{r_0^2}\Big(36 - 18\sin \tilde{\phi}_1 - 431\sin \tilde{\phi}_1^2 + 42\sin \tilde{\phi}_1^3 \\
&- 188\sin \tilde{\phi}_1^4 + 595\sin \tilde{\phi}_1^6 - 240\cos \tilde{\phi}_1 \sin^2 \tilde{\phi}_1 \log\tan\frac{\tilde{\phi}_1}{2}\Big).
\end{aligned} \tag{21}
$$

In the above

$$\frac{\chi_b}{\chi_d} = \frac{1}{1+z_d}\left(\frac{r_s}{\Omega_{\mathrm{m}}}\frac{c^2}{H_0^2}\right)^{1/3}\frac{1}{D_d}, \tag{22}$$

is taken as an additional small parameter no larger than 1st order.

Equations (17), (15) and (16) are three equations relating four variables z_1, r_0, r_1, and $\tilde{\phi}_1$. They can be solve iteratively (four iterations) giving z_1, r_0, and r_1 as functions of $\tilde{\phi}_1$. For an example, to obtain z_1 correct to the first order in β_1, we use Eqs. (17) and (18)

$$z_1 = z_d - (1+z_d)\Delta z^{\mathrm{1st}}(z_d, \tilde{\phi}_1) = z_d + (1+z_d)\beta(z_d)\cos\tilde{\phi}_1, \tag{23}$$

this can be inserted into Eq. (16) to obtain r_1 correct to first order in β_1. This r_1 is then inserted into Eq. (15) (only the lowest order is needed here, i.e., $r_0 = r_1\sin\tilde{\phi}_1$) to obtain r_0 correct to first order. For the next iteration, we include Eq. (19) and the r_s/r_0 term in Eq. (15), and so on. With $z_1(z_d, \tilde{\phi}_1)$, $r_0(z_d, \tilde{\phi}_1)$ and $r_1(z_d, \tilde{\phi}_1)$ in hand, we can compute θ_I, ξ_1, $\Delta\phi$, and α in terms of $\tilde{\phi}_1$ and finally solve the embedded gravitational lensing equation (11) for $\theta_S(\tilde{\phi}_1)$ which can be tabulated to give $\theta_S(\theta_I)$ for a given image.

In Figs. 2 and 3 we have solved the embedded point mass Swiss cheese lens equation (11) and compared the results with those of the conventional Schwarzschild point mass lensing theory. We chose deflector/source redshift respectively $z_d = 0.5$, $z_s = 1.0$, cosmological parameters $\Omega_{\mathrm{m}} = 0.3$, $\Omega_\Lambda = 0.7$, and $H_0 = 70\,\mathrm{km\,s^{-1}\,Mpc^{-1}}$. In Fig. 2, we chose a deflector mass m $= 10^{15}\,M_\odot$ (a rich cluster). For each source angle θ_S, we solved Eq. (11) using the iteration scheme described above obtaining $\tilde{\phi}_1$, z_1, r_0, r_1, θ_I, etc., for both the primary and secondary images. The conventional Schwarzschild results are given by Eq. (6). The impact parameter in conventional lensing is simply taken as $r_{0(\mathrm{Sch})} = \theta_{I(\mathrm{Sch})}D_d$. The dashed/dotted curves are for primary/secondary images, and the solid curve is the fractional correction to the angle between image pairs, i.e., $\theta_{I1} - \theta_{I2}$. The symbol δ is used for the difference between the embedded lens value and the conventional Schwarzschild value. In the left panel, we compute the relative correction in the image position, i.e., $\delta\theta_I/\theta_{I(\mathrm{Sch})}$ (blue-upper bifurcating pair of curves), and the relative correction of the impact parameter r_0, i.e., $\delta r_0/r_{0(\mathrm{Sch})}$, where $\delta r_0 \equiv r_0 - r_{0(\mathrm{Sch})}$ (red-lower bifurcating pair of curves).

In the right panel, we compute the net correction of the bending angle α (central pair of green curves), the effect of the linear correction alone, i.e., $\cos^3\tilde{\phi}_1 - 1$ (lower pair of red curves), and the contribution of the cosmological constant Λ (upper pair of blue curves). Figure 3 is the same as Fig. 2 except that it is for m $= 10^{12}\,M_\odot$ (a typical large galaxy). For
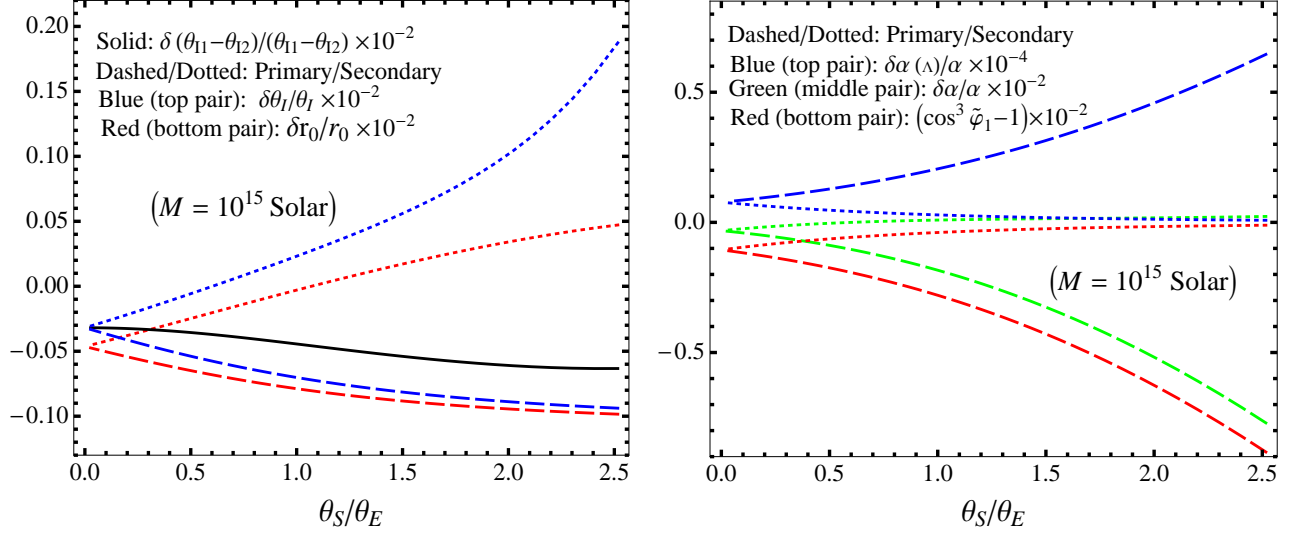
9

FIG. 2. The embedded point mass lens versus the Schwarzschild lens. The deflector/source redshifts are respectively $z_d = 0.5$, $z_s = 1.0$; the cosmological parameters are $\Omega_m = 0.3$, $\Omega_\Lambda = 0.7$, and $H_0 = 70\,\mathrm{km\,s^{-1}\,Mpc^{-1}}$; and the deflector mass is $m = 10^{15}\,M_\odot$. The abscissa θ_S is the source angle measured in units of the classical Einstein ring angle θ_E and the dashed/dotted lines are for primary/secondary images. Quantities being plotted are the fractional differences (represented by a δ) between the conventional Schwarzschild results and the corresponding embedded lens results divided by the conventional results. The bifurcating blue curves are above the corresponding bifurcating red curves. The green bifurcating pair of curves in the right panel are between the upper blue pair and lower red pair. The solid curve in the left panel measures the relative correction of the angle between the primary and secondary images.

$m = 10^{15}\,M_\odot$, corrections in the image angle θ_I can be as large as 0.2%, and corrections in the bending angle α can be as large as -0.8%. For $m = 10^{12}\,M_\odot$, corrections in the image angle θ_I can be as large as 0.01%, and corrections in the bending angle α can be as large as -0.18%. As can be seen from the right panel of Figs 2 and 3, the most important correction is from the linear term, i.e., the $\cos\tilde\phi_1$ correction, the contribution of the next order (Λ term) is at least two orders smaller than the linear correction. We will concentrate on obtaining analytic results for the linear term in the next section.
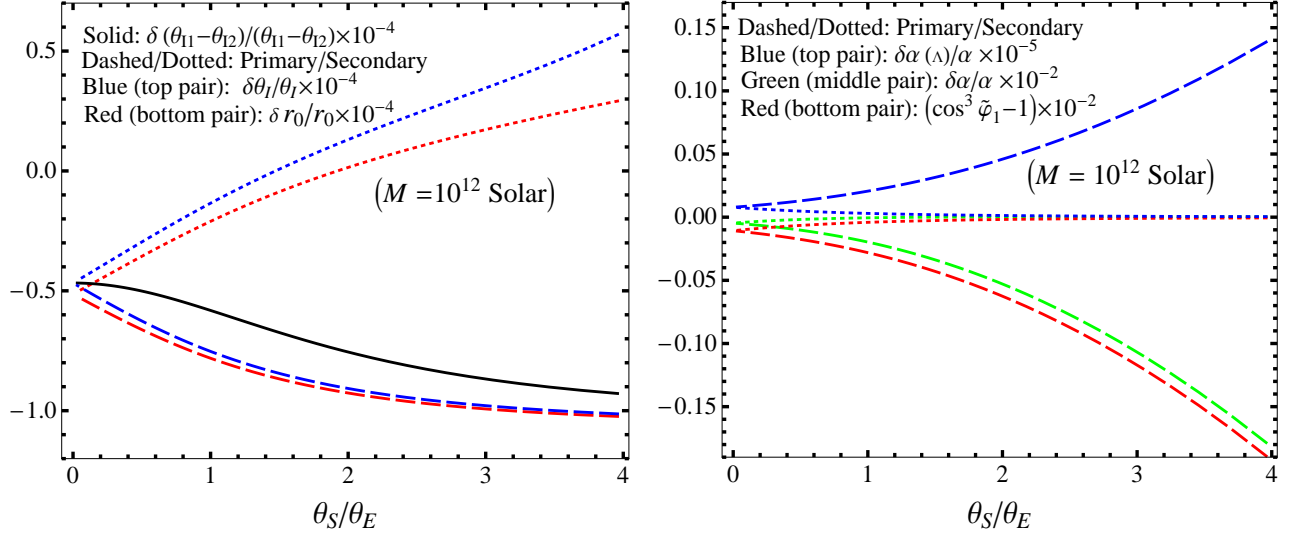
10

FIG. 3. The embedded point mass lens versus the Schwarzschild lens. Same as Fig. 2, except that the deflector mass m $= 10^{12}$ $M_\odot$.

III. IMAGE MAGNIFICATION AND ELLIPTICITY

In this section we include only the lowest order correction to the standard lensing equation caused by the finite range of the embedded point mass Swiss cheese lens. Sereno [20] computes alterations in the magnification but only within the Kottler void. We assume $\sin\theta_I \ll 1$, $\sin\theta_S \ll 1$, and that the Kottler hole is much smaller than the observer-deflector distance, i.e., $g(\tilde{\phi}_1) - 1 \ll 1$, see Eq. (10). From Eq. (5) we obtain

$$\theta_S - \theta_I = -\frac{D_{ds}}{D_s}(-\alpha), \tag{24}$$

which is the same as the standard lens equation (6) except that the bending angle to the lowest order now contains a $\cos^3\tilde{\phi}_1$ factor caused by the finite range of the deflector

$$\alpha = -2\frac{r_s}{r_0}\cos^3\tilde{\phi}_1, \tag{25}$$

see Eq. (32) of [7]. Equation (5) is the form assumed correct by [19] but with a different expression for the deflection angle α.

To lowest order the minimum Kottler impact is

$$r_0 = D_d\theta_I + \mathcal{O}(\beta_1), \tag{26}$$

[see Eqs. (3), (12) and (15)] and the embedded lens equation to lowest order becomes

$$\theta_S - \theta_I = -\frac{\theta_E^2}{\theta_I}\cos^3\tilde{\phi}_1. \tag{27}$$

11

The angle θ_E is the familiar Einstein ring radius

$$\theta_{\mathrm{E}} \equiv \sqrt{2\frac{D_{ds}r_s}{D_dD_s}}, \tag{28}$$

and from Eq. (12) θ_I is related to $\tilde{\phi}_1$ by

$$\sin\tilde{\phi}_1 = \frac{\theta_I}{\chi_b/\chi_d} + \mathcal{O}(\beta_1). \tag{29}$$

This gives us a modified Einstein ring radius (to lowest order)

$$\theta'_{\mathrm{E}} = \sqrt{2\frac{D_{ds}r_s}{D_dD_s}}(\cos\tilde{\phi}_1)^{3/2}, \tag{30}$$

(see [21] for modifications in the Einstein ring within the Kottler void). The two images for
the standard point mass lens are easily found at

$$\theta_I^{\pm} = \frac{1}{2}\left\{\theta_s \pm \sqrt{\theta_s^2 + 4\theta_E^2}\right\}, \tag{31}$$

however, to find the corresponding image positions for the embedded lens you must solve
Eq. (31) with θ_E replaced by θ'_{E}.

The amplification and shear for the embedded lens can be found by a familiar [16] rescaling
$(\theta_S \rightarrow \theta_S/\theta_E \equiv y, \theta_I \rightarrow \theta_I/\theta_E \equiv x)$. Equation (27) simplifies to

$$\mathbf{y} = \mathbf{x} - \frac{\cos^3\tilde{\phi}_1}{x^2}\mathbf{x}, \tag{32}$$

where

$$\sin\tilde{\phi}_1 = \frac{x}{(\chi_b/\chi_d)/\theta_E}. \tag{33}$$

The 2-d Jacobian $A \equiv \partial\mathbf{y}/\partial\mathbf{x}$ is found to be [17]

$$A = \left(1 - \frac{\cos^3\tilde{\phi}_1}{x^2}\right)\begin{bmatrix}1 & 0 \\ 0 & 1\end{bmatrix} + \frac{\cos\tilde{\phi}_1(2 + \sin^2\tilde{\phi}_1)}{x^4}\begin{bmatrix}x_1^2 & x_1x_2 \\ x_1x_2 & x_2^2\end{bmatrix}, \tag{34}$$

which has two eigenvalues

$$a_1 = 1 + \cos\tilde{\phi}_1(1 + 2\sin^2\tilde{\phi}_1)\frac{1}{x^2},$$
$$a_2 = 1 - \cos^3\tilde{\phi}_1\frac{1}{x^2}. \tag{35}$$

Writing

$$A = \begin{pmatrix}1 - \kappa - \gamma_1 & -\gamma_2 \\ -\gamma_2 & 1 - \kappa + \gamma_1\end{pmatrix} \tag{36}$$

12

as is commonly done in standard gravitational lensing theory, we immediately obtain a negative surface mass density

$$\kappa = -\frac{3}{2}\sin^2\tilde{\phi}_1\cos\tilde{\phi}_1\frac{1}{x^2}, \tag{37}$$

and two shear components

$$\gamma_1 = -\cos\tilde{\phi}_1(2+\sin^2\tilde{\phi}_1)\frac{x_1^2-x_2^2}{2x^4},$$
$$\gamma_2 = -\cos\tilde{\phi}_1(2+\sin^2\tilde{\phi}_1)\frac{x_1\tilde{x}_2}{x^4}, \tag{38}$$

with total shear

$$\gamma \equiv \sqrt{\gamma_1^2+\gamma_2^2} = \cos\tilde{\phi}_1(2+\sin^2\tilde{\phi}_1)\frac{1}{2x^2}. \tag{39}$$

The amplification μ for an image is given by

$$\mu^{-1}(\mathbf{x}) = \det A = (1-\kappa)^2 - \gamma^2 = a_1 a_2$$
$$= 1 + 3\cos\tilde{\phi}_1\sin^2\tilde{\phi}_1\frac{1}{x^2} - \cos^4\tilde{\phi}_1(1+2\sin^2\tilde{\phi}_1)\frac{1}{x^4}.$$

The image of a circular source (eccentricity $\epsilon = 0$) will be an ellipse of eccentricity

$$\epsilon = \sqrt{1-\frac{a_2^2}{a_1^2}} = \frac{\sqrt{(2x^2+3\sin^2\tilde{\phi}_1\cos\tilde{\phi}_1)(2+\sin^2\tilde{\phi}_1)\cos\tilde{\phi}_1}}{x^2+\cos\tilde{\phi}_1(1+2\sin^2\tilde{\phi}_1)}. \tag{40}$$

The standard lensing results are obtained by putting $\cos\tilde{\phi}_1 = 1$ and $\sin\tilde{\phi}_1 = 0$ in the above. Deviations from standard image amplification μ and the image ellipticity ϵ caused by embedding are shown in Fig. 4. The left panel is for a deflector mass m $= 10^{15}\,M_\odot$ and the right is for m $= 10^{12}\,M_\odot$. In each plot, the red solid and the (identical to accuracy shown) black dotted (upper) curves show the corrections in ellipticity, i.e., $\delta\epsilon/\epsilon$ for the primary and secondary images. The solid blue (lower) curve is the relative correction in the magnification ratio, i.e., $\delta(\mu_1/\mu_2)/(\mu_1/\mu_2)$. For the m $= 10^{15}\,M_\odot$ case, the correction in ellipticity can be as large as 0.03%, and the correction in magnification ratio can be as large as -0.17%. For the m $= 10^{12}\,M_\odot$ case, the correction in ellipticity can be as large as 0.004%, and the correction in magnification ratio can be as large as -0.019%.

These lowest order shielding effects, i.e., no bending outside the Kottler void, are far larger than approximation errors in the standard linear theory caused by assuming the photon's path is infinite. The classical Einstein bending angle $4M/r$ depends only on the impact parameter r and not the comoving source/deflector distances χ_s or χ_d because it is
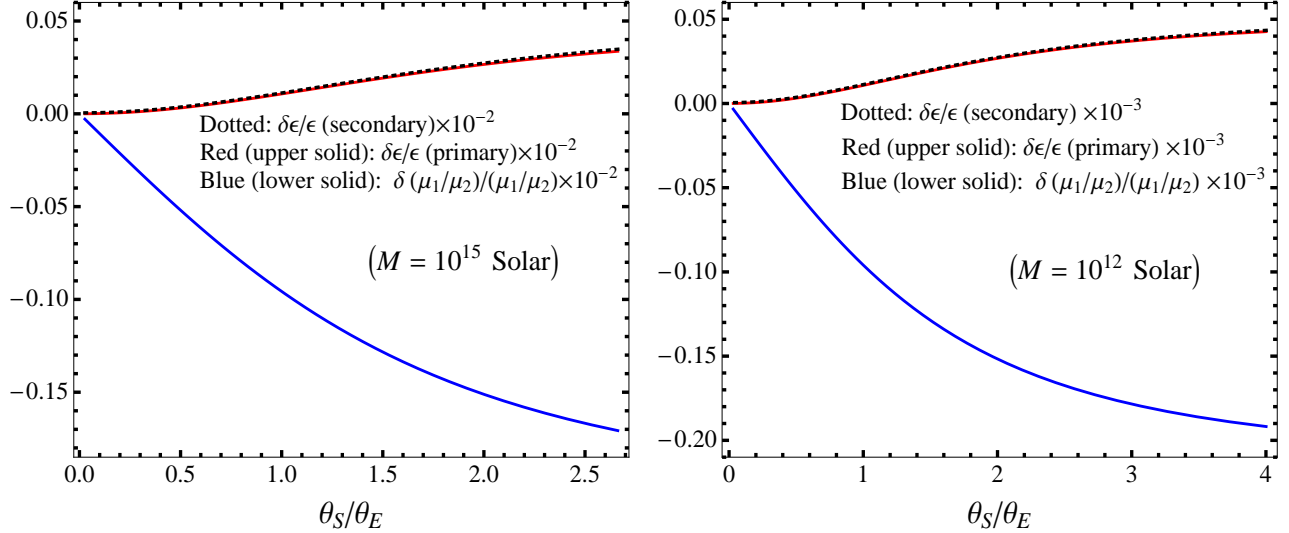
FIG. 4. Linear corrections to Schwarzschild lensing caused by the finite range of embedding— the magnification ratio μ_1/μ_2 and the ellipticity ϵ are plotted as a function of source position. The cosmological parameters and redshifts are same as in Figs. 2 and 3.

obtained by integrating from $-\infty$ to $+\infty$ along an approximated photon trajectory. The effect of finite integration along the line of sight in standard lensing does make the bending angle smaller but only by terms of order $[r/\chi_d]^2$ and $[r/(\chi_s - \chi_d)]^2$. Because bending occurs only within the Kottler hole, our lowest order correction, i.e., the $1 - (\cos\phi)^3$ term, is much larger than the angle reduction caused by excluding bending in conventional theory beyond a distant source and observer. Our $\cos\phi$ correction is of order $[r/\chi_b]^2$ where χ_b is the comoving size of the Kottler hole and is significantly smaller than χ_d and $(\chi_s - \chi_d)$. For an example, assume $M = 10^{12} M_\odot$, $z_d = 0.5$, and same cosmological parameters as used in the paper, we found $\chi_b/\chi_d = 9.54 \times 10^{-4}$. Therefore, the effect of finite line of sight integration is $\sim 10^{-7}$ order smaller than the lowest order corrections predicted in current paper, and $\sim 10^{-4}$ order smaller than the Λ correction (refer to the right panel of Fig. 3).

IV. CONCLUSIONS

We have given a lens equation (5) valid for use on highly concentrated lenses (point masses) which are embedded into the otherwise spatially homogeneous and flat background FLRW cosmology. We have also given the additional equations necessary to iteratively solve

this embedded lens equation and have outlined a procedure for doing so. As an example we have looked at differences in strong lensing predictions made by this new theory as compared to the conventional theory. We used a large galaxy size lens (m $= 10^{12}$ $M_\odot$) and a rich cluster size lens (m $= 10^{15}$ $M_\odot$) and found, as was suggested before in [7, 9], that predictions for strong lensing effects made by embedded lens theory differs by less than 1% from predictions made by the conventional theory. In Section II we looked at image angle differences and in Section III we looked at lowest order analytic expressions for image magnification and ellipticity differences. We expect more significant effects to occur for weak lensing applications where impact distances are much larger and where shielding effects ($\cos^3 \tilde{\phi}_1$) are more significant.

We have found that embedding affects time delays, image positions, magnifications and ellipticities differently than does the presence of substructure. For example, substructure has a large effect on magnification, but has almost no effect on the time-delay; our model predicts corrections in magnifications and even larger corrections in the time delays. The small size of the effect of embedding on magnification and ellipticity in strong lensing $\sim 0.1\%$ that we have found here is an order of magnitude smaller than we have found on time delays in strong lensing $\sim 4\%$ (Chen et. al. 2010). Knowing this is important to all standard lensing calculations; you only make a small embedding error using the standard theory when you use it for strong lensing magnification and ellipticity calculations; not so for time delays or for weak lensing applications. However, because of the size of the effect, embedding differences can only be tested when we have better knowledge of lens mass distributions. Some current observations (such as Hubble observations of lens image positions) are accurate enough to resolve the embedding corrections we predict; however, degeneracy in mass modeling currently prohibits confirmation. As soon as the mass models are appropriately accurate, embedding effects can be tested.

An additional special feature presented by this model is the analytic dependence of lensing on the cosmological constant Lambda. This model absolutely settled the argument about how the cosmological constant effects lensing. Prior to its use many from the astrophysics community believed that the cosmological constant did not affect lensing at all, even though the GR community argued that it must (see [10, 18–20]). The exact analytic nature of the dependence was in dispute prior to the introduction of this model. For example the most significant effect of the cosmological constant on the bending angle appears in square-root

terms (see equations such as (32) of [7]) and is an order of magnitude larger effect than previously estimated. All other work also missed the most significant effect of embedding on lensing, the shielding effect. Because the range of a real lens is not finite, this model becomes useful when 0.5% accuracy in strong lensing deflection angles is desired or when 5% accuracy in time delays is required or when 5% accuracy in weak lensing deflection angles is required.

[1] A. Einstein & E. G. Straus, Rev. Mod. Phys., 17, 120 (1945).

[2] E. Schücking, Z. Phys., 137, 595 (1954).

[3] R. Kantowski, Astrophys. J., 155, 89 (1969).

[4] C. C. Dyer & R. C. Roeder, Astrophys. J., 189, 167 (1974).

[5] T. Schücker, Gen. Relativ. Gravit., 41, 67 (2009).

[6] F. Kottler, Ann. Phys. (Leipzig), 361, 401 (1918).

[7] R. Kantowski, B. Chen & X. Dai, Astrophys. J., 718, 913 (2010).

[8] R. Kantowski, T. Vaughan & D. Branch, Astrophys. J., 447, 35 (1995).

[9] B. Chen, R. Kantowski & X. Dai, Phys. Rev. D, 82, 043005 (2010).

[10] W. Rindler & M. Ishak, Phys. Rev. D, 76, 043006 (2007).

[11] T. Schücker, Gen. Relativ. Gravit., 41, 1595 (2009).

[12] T. Schücker, arXiv:1006.3234 (2010).

[13] K.-E. Boudjemaa, M. Guenouche & S. R. Zouzou, Gen. Relativ. Gravit., 43, 1707 (2011).

[14] M. Ishak, W. Rindler & J. Dossett, Mon. Not. R. Astron. Soc., 403, 21521 (2010).

[15] M. Ishak & W. Rindler, Gen. Relativ. Gravit., 42, 2247 (2010).

[16] P. Schneider, J Ehlers & E. E. Falco, *Gravitational Lenses* (Springer-Verlag, Berlin, 1992).

[17] R. R. Bourassa & R. Kantowski, Astrophys. J., 195, 13 (1975).

[18] M. Ishak, Phys. Rev. D, 78, 103006 (2008).

[19] M. Sereno, Phys. Rev. Lett., 102, 021301 (2009).

[20] M. Sereno, Phys. Rev. D, 77, 043004 (2008).

[21] M. Ishak, W. Rindler, J. Dossett, J. Moldenhauer & C. Allison, Mon. Not. R. Astron. Soc., 388, 1279 (2008).